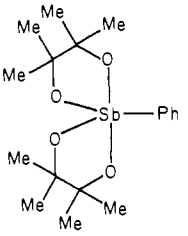

14, 13 (12.1)

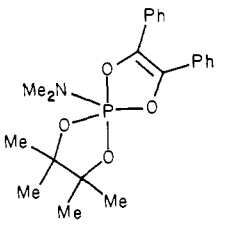

15, 31

spectively, for pseudorotation which has the phenyl group apical and one of the rings diequatorial in an intermediate trigonal bipyramid.[37]

We conclude that the basic structural principles developed for phosphorane stereochemistry[2,3,38] apply to the stereochemistry of pentacoordinated arsenic compounds and apparently also to pentacoordinated antimony.[39,40] The ease of attainment of the rectangular-pyramidal geometry appears to be reflected in the relative fluxional character assigned to these elements in their pentacoordinated state.[5]

Acknowledgment. The support of this research by the National Science Foundation (Grant CHE 79-10036) is gratefully acknowledged. We also thank the University of Massachusetts Computing Center for generous allocation of computer time.

Registry No. 5, 79677-99-9; **6**, 72409-78-0.

Supplementary Material Available: Compilations of observed and calculated structure factor amplitudes and thermal parameters (Tables A and B), parameters for hydrogen atoms (Tables C and D), and least-squares planes (Tables E and F) for **5** and **6**, respectively (26 pages). Ordering information is given on any current masthead page.

(35) Casey, J. P.; Mislow, K. *J. Chem. Soc., Chem. Commun.* **1970**, 1410.
(36) Wieber, M.; Baumann, N. *Z. Anorg. Allg. Chem.* **1975**, *418*, 279.
(37) Reference 3, p 163.
(38) Recently, we discovered the first discrete rectangular pyramids for the group 4A elements Si, Ge, and Sn (Harland, J. J.; Day, R. O.; Vollano, J. F.; Sau, A. C.; Holmes, R. R. *J. Am. Chem. Soc.* **1981**, *103*, 5269. Sau, A. C.; Day, R. O.; Holmes, R. R. *Ibid.* **1980**, *102*, 7972; **1981**, *103*, 1264, respectively). Pentacoordinate principles regarding the stereochemistry of group 4A elements also are very similar to those for phosphoranes (Day, R. O.; Holmes, J. M.; Sau, A. C.; Holmes, R. R. *Inorg. Chem.* **1982**, *21*, 281. Sau, A. C.; Day, R. O.; Holmes, R. R. *Ibid.* **1981**, *20*, 3076).
(39) In view of the trigonal-bipyramidal structures for **14**,[33] (*p*-tolyl)$_5$Sb (Brabant, C.; Hubert, J.; Beauchamp, A. L. *Can. J. Chem.* **1973**, *51*, 2952), and the cyclohexane solvate, $Ph_5Sb{\cdot}0.5C_6H_{12}$ (Beauchamp, A. L. *J. Organomet. Chem.* **1974**, *82*, 231), it is felt that the square-pyramidal structure of Ph_5Sb (Wheatley, P. J. *J. Chem. Soc.* **1964**, 3718; Beauchamp, A. L.; Bennett, M. J.; Cotton, F. A. *J. Am. Chem. Soc.* **1968**, *90*, 6675) is a result of lattice effects. Strong support for this assertion results from calculations showing that the most fluxional pentacoordinated member of the group 5A elements, antimony(V), can be stabilized by lattice effects in a square-pyramidal geometry (Brock, C. P. *Acta Crystallogr., Sect. A* **1977**, *A33*, 898).
(40) Reference 2, p 10.

Vibrational Fine Structure in the Valence Ionizations of Transition-Metal Hexacarbonyls: New Experimental Indication of Metal-to-Carbonyl π Bonding

John L. Hubbard and Dennis L. Lichtenberger*

Contribution from the Department of Chemistry, University of Arizona, Tucson, Arizona 85721.
Received June 29, 1981

Abstract: The first observations of metal–carbon vibrational structure in photoionization bands are reported. Attention is focused on the predominantly metal d ionizations of $M(CO)_6$ (M = Cr, Mo, and W), and the methods for obtaining high resolution and very high signal-to-noise He I ionization data are detailed. The $^2T_{2g}$ ionization band of $Cr(CO)_6$ and the spin–orbit split $^2E''$ and $^2U'$ bands of $W(CO)_6$ show distinct vibrational progressions which correspond to the totally symmetric (a_{1g}) metal–carbon stretching mode in the positive ion states. The metal–carbon stretching frequencies are found to be significantly less in the positive ion states than in the ground states, indicating a reduction of metal–carbon bond order upon the loss of a t_{2g} electron. Evaluation of the vibrational progressions shows that the metal–carbon bond length increases on the order of 0.10 Å upon t_{2g} ionization in the case of $W(CO)_6$ and about 0.14 Å in the case of $Cr(CO)_6$. In addition, the beginning of a short progression in the a_{1g} carbon–oxygen stretching mode is observed in the $Mo(CO)_6$ spectrum and is clearly seen in the $W(CO)_6$ spectrum. All of these observations show that removal of an electron from the predominantly metal t_{2g} orbitals, which are strictly π symmetry with respect to the carbonyls, substantially weakens the metal-to-carbonyl bond.

The synergic bonding model is one of the most fundamental and pervasive concepts in the description of transition-metal–ligand interactions.[1] A commonly invoked example is the bonding of a carbonyl ligand with a transition metal, in which the σ donation by the carbonyl is described as being accompanied by π back-donation from the metal. The significance of this interaction continues to prompt many theoretical studies at varying levels of sophistication.[2-5] In general, the calculations have been consistent with the π back-bonding scheme, although a lack of clarity in evaluation of the π interaction has led to some confusion concerning its relative magnitude.[4] Considerable indirect experimental support for this scheme has been provided by the interpretation of vibrational,[6,7] mass spectrometric,[8] and core level XPS[9] data,

(1) Cotton, F. A.; Wilkinson, G. "Advanced Inorganic Chemistry", 4th ed.; Wiley-Interscience: New York, 1979.
(2) Hillier, I. H.; Saunders, V. R. *Mol. Phys.* **1971**, *22*, 1025-1034.
(3) Bursten, B. E.; Freir, D. G.; Fenske, R. F. *Inorg. Chem.* **1980**, *19*, 1810-1811.
(4) Hall, M. B.; Sherwood, D. E. *Inorg. Chem.* **1980**, *19*, 1805.
(5) Larsson, S.; Braga, M. *Int. J. Quantum Chem.* **1979**, *15*, 1-5.
(6) Cotton, F. A.; Kraihanzel, C. S. *J. Am. Chem. Soc.* **1962**, *84*, 4432-4438.
(7) Jones, L. H.; McDowell, R. S.; Goldblatt, M. *Inorg. Chem.* **1969**, *8*, 2349-2363.
(8) Svec, H. J.; Michels, G. D.; Flesch, G. D. *Inorg. Chem.* **1980**, *19*, 479-485.

0002-7863/82/1504-2132$01.25/0

to name just a few. However, by the nature of the synergic interaction, most experiments are not able to clearly separate the σ- and π-bonding effects. The uncertainties have contributed to the continuing discussion of this bonding.

At the simplest level, the bonding nature of an electron in an orbital can be assessed in terms of its effect on specific interatomic distances and angles. By first principles, if removing an electron from a particular orbital lengthens the bond distance between two particular atoms, then that orbital is understood to have a bonding effect between those atoms. This approach is commonly used when the orbital of interest is the HOMO, as long as the crystal structure of both the parent molecule and the oxidized molecule can be determined. Much the same structural information can be obtained from photoelectron spectroscopy if the vibrational progression associated with the ionization (oxidation) is resolved.[10-12] This technique is not limited to ionization from the HOMO. Franck–Condon evaluation of the vibrational intensity pattern provides the quantitative indication of the geometry changes caused by removal of the electron. Qualitatively, if the orbital electron is essentially nonbonding and no geometry change occurs with ionization, then the most intense (vertical) ionization will be to the lowest vibrational level in the positive ion (adiabatic), and ionization intensity to the higher vibrational levels will be small in comparison. If a bond length or geometry does change significantly with the ionization, then a vibrational progression will result with the most intense transition to a higher vibrational quantum level. Furthermore, the frequency spacing of the progression will indicate whether the electron was bonding or antibonding with respect to the normal mode nuclear displacements.

Vibrational progressions are most commonly observed in the ionization spectra of small molecules. In larger molecules the resolution of discrete vibrational modes in an ionization band may be thwarted by the complicated overlap of many fundamental vibrational modes activated upon ionization. Molecules that have low-frequency fundamental modes, like the metal carbonyls, are especially likely to have vibrational detail so closely spaced that spectral resolution is beyond most instrumental capabilities. In this paper we demonstrate for the first time the ability of high-resolution UPS to detect metal–carbon vibrational fine structure in the ionization bands of metal carbonyls. Details of the experimental procedure and spectral analysis techniques are presented. We focus attention in this paper on the t_{2g} ionizations of $Cr(CO)_6$, $Mo(CO)_6$, and $W(CO)_6$. These molecules are generally excellent prototypes for theoretical and experimental study of metal–carbonyl bonding because of their high symmetry and are valuable to the present study because the metal t_{2g} orbitals have pure π interaction with the carbonyls. These molecules are also attractive because of their good stability and volatility. Their normal mode vibrational behavior has previously been examined[3] and allows detailed evaluation of the vibrational progressions. The experimental information is sufficient to provide a quantitative determination of the metal–carbon bond length in the positive ions and has important implications concerning the electronic interactions in these complexes.

Experimental Section

The photoelectron spectra presented in this paper were obtained with a modified GCA–McPherson ESCA-36 spectrometer. Because of the special nature of these observations, it is appropriate to describe the modifications and data collection procedures in some detail. Detection of the ionization features presented in this paper requires good resolution, a high signal-to-noise ratio, controlled stability of the spectrometer, and data collection and analysis procedures that are not normal to this area of spectroscopy. The He I radiation was generated by a water-cooled capillary-discharge lamp mounted in a two-stage differential pumping section. All spectra were internally calibrated to the $^2P_{3/2}$ ionization of argon (15.76 eV), which was introduced simultaneously with the sample into the instrument. Typical sensitivity over the argon line was greater than 10^5 counts per second with an argon pressure less than 10^{-5} torr measured near the analyzer. Resolution of the argon reference line was maintained at 0.015–0.018 eV *during* the data acquisition on each sample. The kinetic energy scale was calibrated with a CH_3I (9.55 eV)/Ar (15.76 eV) gas mixture prior to data collections, and it was found that the scale expansion did not change during data acquisition on our instrument.

The measured kinetic energy for a given spectral feature can shift during an experiment for a variety of reasons, and the reduction and precise control of these shifts are among the more important factors in observing the subtle ionization features. First, it is important to maintain steady pressures in the ionization region. Argon pressure was controlled by a Granville-Phillips variable leak valve, and the sample pressure was controlled by a stainless steel needle valve. In addition, slight changes in the temperature or the surface conditions on sensitive instrument components (slits and sample chamber are most important) will cause the spectrum to drift and will obscure small spectral details. We control this drift through a data collection procedure that utilizes the argon $^2P_{3/2}$ ionization as an internal spectrum "lock" rather than just a reference line. All spectra reported in this study were collected with the kinetic energy scale drift controlled to less than 0.005 eV. For a typical experiment the spectrum is collected in 300 data channels over a 1.0–1.2-eV window. A short data scan (0.5–5.0 min depending on instrument stability) is followed by a scan of the Ar signal (6 s), and any drift of the kinetic energy scale is corrected by computer control. These data scans are accumulated to a total of 8–12 s/channel. It was found necessary to modify the PDP-8e to store data in double precision (24 bits) to prevent systematic round-off errors that can occur at the high signal-to-noise level of our experiments. After several hours of continuous, uninterrupted operation of the instrument, the conditions stabilize sufficiently so that long, single-scan collections (5–15 s/channel) may be obtained with the drift less than 0.005 eV. The spectral fine structure was shown to be invariant to the specific collection procedure. Twelve independent data collections were obtained for $Cr(CO)_6$, five for $Mo(CO)_6$, and ten for $W(CO)_6$.

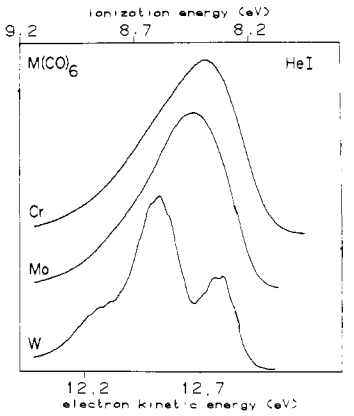

Figure 1. He I photoelectron spectra of $Cr(CO)_6$, $Mo(CO)_6$, and $W(CO)_6$.

Table I. Ionization Energies of the Group 6 Hexacarbonyls[a]

method	parameter	$Cr(CO)_6$	$Mo(CO)_6$	$W(CO)_6$
mass spec[8]	IE	8.42 (3)	8.46 (1)	8.60 (2)
UPS, Lloyd et al.[15]	IE	8.40 (2)	8.50 (2)	8.56 (2) $^2U'$ 8.30 $^2E''$
UPS, this work	IE	8.40 (1)	8.45 (1)	8.59 (1) $^2U'$ 8.33 (1) $^2E''$
	W^b	0.47	0.42	0.23 $^2U'$ 0.16 $^2E''$
	η^c	0.39	0.33	0.10 $^2U'$ 0.08 $^2E''$

[a] In eV. Standard deviations in parentheses where shown. [b] Full widths of the peaks at half-heights. [c] Asymmetry parameter, η, defined as $(W_H - W_L)/(W_H + W_L)$, where W_H and W_L are the widths for the high and low binding energy halves of the band.

Results

Figure 1 shows the ionization bands corresponding to the t_{2g} ionizations of $Cr(CO)_6$, $Mo(CO)_6$, and $W(CO)_6$. The vertical

(9) Barber, M.; Connor, J. A.; Hillier, I. H.; Saunders, V. R. *J. Chem. Soc., Chem. Commun.* **1971**, 682.
(10) Turner D. W.; Baker, C.; Baker, A. D.; Brundle, C. R. "Molecular Photoelectron Spectroscopy"; Wiley-Interscience: New York, 1970.
(11) Rabalais, J. W. "Principles of Ultraviolet Photoelectron Spectroscopy"; Wiley: New York, 1977.
(12) Eland, J. H. D.; Danby, C. J. *Int. J. Mass Spectrom. Ion Phys.* **1968**, *1*, 111–119.

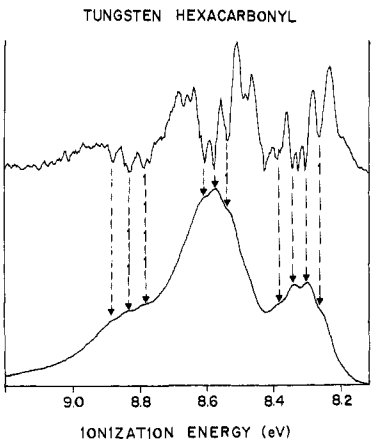

Figure 2. Absolute value of the first derivative of the $W(CO)_6$ band plotted above the ionization band. The arrows show the visual enhancement of the vibrational features.

ionization energies are listed in Table I and are compared with data from other investigations. It is interesting to note that the ionization energies determined by mass spectrometry[4] are not true adiabatic energies, but correspond most closely to our vertical ionization energies (band maxima) for $Cr(CO)_6$ and $Mo(CO)_6$ and to the vertical ionization energy of the second main peak ($^2U'$ state) for $W(CO)_6$.

In the case of $W(CO)_6$, the fine spectral detail caused by the vibrational progressions is clearly observed in Figure 1. This figure, which is the normal method of displaying photoelectron ionizations, is not adequate for visually detecting the fine structure in the $Cr(CO)_6$ and $Mo(CO)_6$ spectra. In these cases the important spectral features due to the vibrations are small in comparison to the total intensity of the band. Clear observation of such features is commonly accomplished in other spectroscopies by examination of the derivative spectrum[13] or Fourier analysis,[14] and we have adopted these techniques to clarify the structure in these ionizations. In order to demonstrate the usefulness of such techniques for analyzing high signal-to-noise UPS data, we will first examine the $W(CO)_6$ ionization in detail.

A. $W(CO)_6$. The $W(CO)_6$ t_{2g} ionization envelope is characterized by two major bands in an approximately 2:1 ratio. These bands have been observed by Lloyd et al.[15] and are understood in terms of the large spin–orbit coupling of the W atom, which splits the sixfold degenerate $^2T_{2g}$ ion state (t_{2g}^5) to a fourfold degenerate $^2U'$ state and a twofold degenerate $^2E''$ state. A shoulder on the high ionization energy side of the $^2U'$ band is also clearly observed. The shoulder is separated by 2090 cm^{-1} from the main ionization, as determined by curve fitting with program GFIT[16] (half widths of asymmetric bands constrained to be equal). This shoulder was poorly resolved by Lloyd et al.,[15] who correlated it to a short progression of the t_{1u} carbon–oxygen stretching mode at 1998 cm^{-1}. Our spectrum not only shows this shoulder very clearly but also shows smaller detail on top of the shoulder as well as on the $^2E''$ and $^2U'$ bands. We will focus primary attention on this smaller detail, which will be shown to correspond to metal–carbon stretching. It should be pointed out that these same features have also been observed with a Varian IEE-15 photoelectron spectrometer.[17]

First Derivative Analysis. The first derivative of the $W(CO)_6$ spectrum is shown above the original spectrum in Figure 2. The absolute value of the derivative has been plotted to facilitate the location of the minimum slopes on the spectrum. The visibility

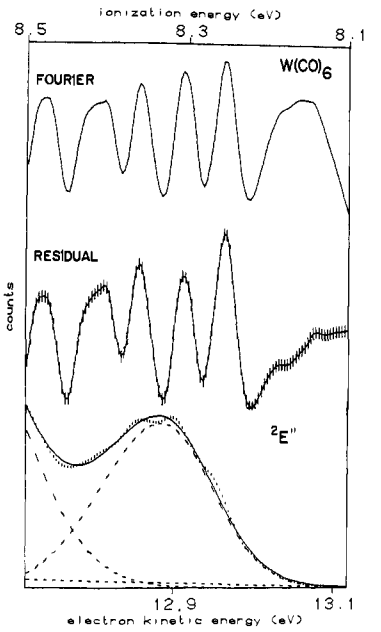

Figure 3. Residual and Fourier analysis of the $^2E''$ ionization of $W(CO)_6$. The lower plot is the experimental data (dots) fit with the broad Gaussians on a base line (dashed lines) giving the solid line.

Table II. Vibrational Frequencies (cm^{-1}) as Determined by Derivative, Residual, Fourier, and Simulation Analysis[a]

	derivative	residual	Fourier	simulated	ν_2, neutral (gas phase)[3]
$W(CO)_6$	327 (10)	404 (6)	418 (1)	387	426
$Cr(CO)_6$	331 (20)	317 (60)	310 (43)		379

[a] Standard deviations are in parentheses.

of the fine structure is greatly enhanced by this technique and allows us to more systematically determine the vibrational spacings.

Residuals of Fit Analysis. When relatively small features are resolved on the surface of a large broad band, it is useful to remove the bulk of the band so as to enhance the visibility of the finer detail. Figure 3 illustrates this process for the $^2E''$ band of $W(CO)_6$. The basic shape of the band is fit with a broad Gaussian band by using the program GFIT.[17] The residuals are then determined as a point-by-point difference between the fit curve and the data. The plot of the residuals shows the net pattern of the smaller features that were somewhat obscured by their previous superposition on the overall ionization envelope.

It should be noted that this technique is good for visual enhancement of the fine spectral detail but is not necessarily adequate for determining the energy spacings. This is because the residual amplitudes are the differences between the data and the smooth fit curve, and the maximum residuals do not necessarily occur at the exact centers of the vibrational components. For the same reasons, the intensities of the residuals do not reflect the intensities in the vibrational progression. These points are also important for understanding the Fourier transform analysis.

Fourier Transform Analysis. The Fourier transform process is an alternative to the residuals of fit analysis. In this process the ionization band, thought of as being in the time domain, is transformed to a function in the frequency domain by way of standard Fourier techniques.[14] The low "frequency" components (low values of $1/E$ corresponding to the broad shape of the overall ionization band) can then be "filtered" or removed. The inverse transform is then performed to return the data to the time domain. The Fourier plot in Figure 3 shows the peak fine structure without the low-frequency structure. Comparison of the Fourier analysis to the residuals of fit analysis illustrates the striking similarity of the techniques. This emphasizes that the Fourier analysis is expected to be subject to the same errors in peak positions and

(13) Cahill, J. E.; Padera, F. G. *Am. Lab.* (*Fairfield, Conn.*) **1980**, *12*, 101–112.
(14) Stanley, W. D.; Peterson, S. J. *BYTE* **1978**, December, 14–25. Fourier transforms were performed by direct application of the mathematical functions presented in this reference.
(15) Higginson, B.; Lloyd, D. R.; Burroughs, P.; Gibson, D. M.; Orchard, A. F. *J. Chem. Soc., Faraday Trans. 2*, **1973**, *69*, 1659.
(16) Lichtenberger, D. L.; Fenske, R. F. *J. Am. Chem. Soc.* **1976**, *98*, 50.
(17) Lichtenberger, D. L. Ph.D. Thesis, University of Wisconsin, 1974.

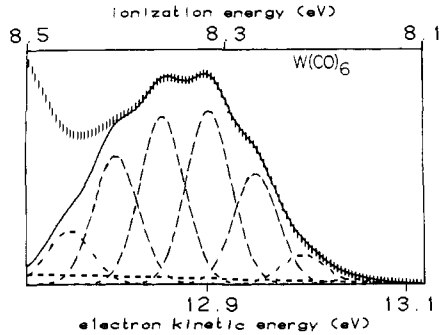

Figure 4. The $^2E''$ band fit with a progression of symmetric, evenly spaced component bands. The vertical dashes are the experimental data. The dashed lines are the vibrational components and base line, and the solid line is the fit sum.

intensities mentioned for the residuals process.

Spectral Simulation. The $^2E''$ ionization band was also simulated with a progression of evenly spaced symmetric and equal width bands, as would be expected for a partially resolved vibrational progression. The $^2E''$ band was chosen for this simulation because it is least complicated by overlap with other ionization features. Figure 4 shows that the simulation is very good. The peaks are evenly spaced at 387 cm^{-1} and fall into a nearly Gaussian intensity pattern.

The frequencies obtained from the different spectral analysis techniques are summarized in Table II. The frequency obtained by simulation is relatively free of the errors encountered by the derivative, Fourier, and residuals analyses. It serves as a warning for indiscriminantly using these other techniques for determining peak positions and separations. Direct comparison of the simulated $^2E''$ band spacings to those indicated by the derivative analysis shows the derivative to considerably underestimate the spacings. This is a result of the closely overlapping bands merging together, particularly around the band maximum. The derivative spacings along the side of the band are more similar to those of the simulated band elements. For similar reasons, the residual of fit and Fourier analyses tends to overestimate the spacings around the band maximum.

B. $Cr(CO)_6$. The $Cr(CO)_6$ $^2T_{2g}$ band is not dramatically split by spin–orbit coupling like the $W(CO)_6$ band because of the much smaller spin–orbit coupling parameter for the Cr atom ($\lambda \simeq 0.027$ eV).[18] One important observation is that the overall width of the single $Cr(CO)_6$ band is as broad as both the major $W(CO)_6$ peaks together. Also, the small fine structure directly observed on the $W(CO)_6$ peaks is not apparent upon visual inspection of the $Cr(CO)_6$ band as plotted in Figure 1. However, this ionization band was consistently reproduced within the width of the plotted line in Figure 1, and the essential vibrational detail is clearly found from inspection of the $Cr(CO)_6$ data in terms of the derivative, Fourier, or residual spectra.

Figure 5 shows the first derivative of the $Cr(CO)_6$ band. This derivative spectrum was also consistently obtained in 12 independent data collections. It shows a simple progression of six to seven components with a frequency spacing of 330 cm^{-1} (Table II). The progression is most clearly seen on the low ionization energy side of the band. Figure 6 shows the plots of the Fourier and residual analyses for the $Cr(CO)_6$ data. The frequencies determined by these methods (Table II) are in close agreement with the derivative analysis, indicating the consistency of the three techniques when the inflections caused by the progression lie on a more or less constant slope of the overall band.

C. $Mo(CO)_6$. The spectrum of the $Mo(CO)_6$ $^2T_{2g}$ band is shown in Figure 1. The single band is somewhat more narrow than the $Cr(CO)_6$ band and shows no visibly distinct small fine structure as in the $W(CO)_6$ spectrum. The application of the derivative, residual, and Fourier techniques previously described gives evidence of vibrational structure, but not in the form of a simple extended harmonic progression. Reasons for this will be discussed. One broad, gentle inflection on the high BE side is discernible, however. The derivative confirms the presence of this inflection at approximately 2000 cm^{-1} from the peak maximum. This feature is similar to the high BE shoulder observed on the $W(CO)_6$ $^2U'$ peak.

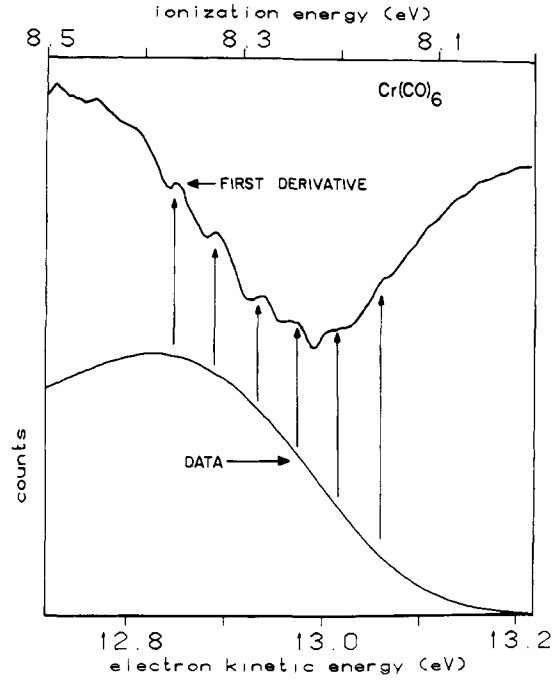

Figure 5. First derivative of the $Cr(CO)_6$ spectrum.

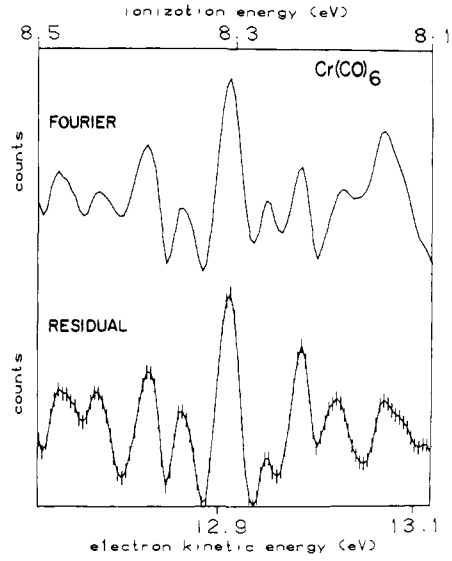

Figure 6. Fourier and residual analysis of the $Cr(CO)_6$ spectrum.

Interpretation of the Vibrational Progressions

A. $W(CO)_6$. Assignment and interpretation of the vibrational progressions in these ionizations are straightforward for these high-symmetry metal hexacarbonyl complexes. The vibronic selection rules for UPS transitions[19] together with the measured frequencies give a clear indication of the primary fundamental stretching modes that are being excited in the ionization process. The shoulder on the high ionization energy side of the $^2U'$ band of $W(CO)_6$ represents the beginning of a short progression with a frequency of $\approx$2100 cm^{-1} in the positive ion, which corresponds closely with the ν_1 (a_{1g}) fundamental stretching frequency in the

(18) Griffith, J. S. "The Theory of Transition Metal Ions"; University Press: Cambridge, 1961.

(19) Herzberg, G. "Molecular Spectra and Molecular Structure"; D. Van Nostrand: New York, 1966; Vol. III, Chapter 2, pp 150–155.

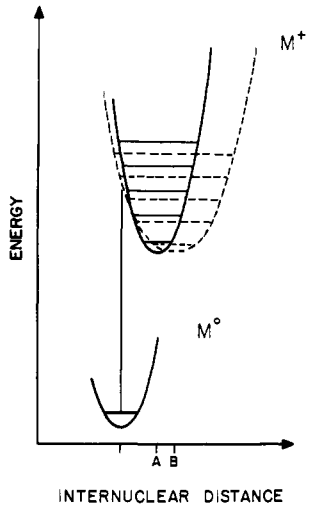

Figure 7. Potential well description of the Franck–Condon principles. (A) represents displacement based on the assumption that both ground and positive ion states have identically shaped potential wells (solid M^+ line). (B) represents displacement assuming a broader and more shallow positive ion well (dashed M^+ line).

neutral molecule at 2126 cm^{-1}. The relative nuclear motions of this normal vibration in the neutral molecule are shown in **1**

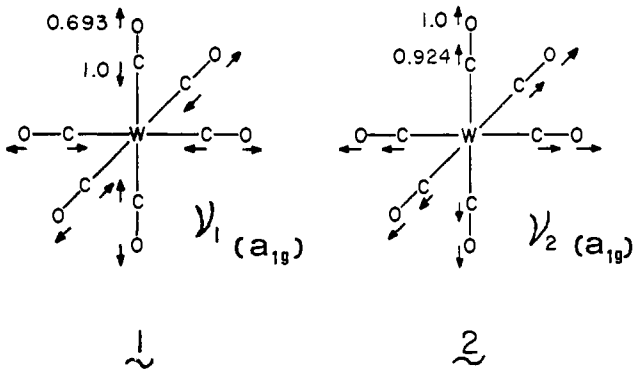

(relative displacements indicated). This mode is identified as the totally symmetric, primarily carbon–oxygen stretch. The $^2E''$ band and the $^2U'$ band, as well as the high ionization energy shoulder on this band, all show a three to five element progression with spacing of ~390 cm^{-1}. This spacing corresponds to the ν_2 (a_{1g}) mode (**2**), which is identified as the totally symmetric metal–carbon stretching mode.

The frequency of ν_2 in the positive ion state (390 cm^{-1}) is significantly less than the frequency in the neutral molecule (426 cm^{-1}). This is one indication from the experimental data that removal of an electron from the predominantly metal d t_{2g} orbitals reduces the bond strength between the metal and the carbonyls. The second evidence comes from the intensity pattern in the ν_2 progression, which is most clearly displayed in Figure 4. The most intense ionization is not to the lowest ν_2 (a_{1g}) vibrational quantum level ($v = 0$), as it would be for removal of a strictly nonbonding electron and no change in bond distance. Rather, the most intense ionization is to at least the $v = 3$ vibrational quantum level, which means that the metal–carbon vibrational potential well in the positive ion state has shifted with respect to that in the ground state. This is illustrated qualitatively in Figure 7. Thus the intensity pattern indicates a metal–carbon bond distance in the positive ion considerably different from that in the neutral molecule.

The magnitude of the change in the metal–carbon distance with removal of one t_{2g} electron is determined from a normal Franck–Condon analysis[12] of the vibrational structure in the ionization. For correct quantitative treatment of the relative motion of each nucleus in the normal vibrational mode, we have reconstructed the **F**, **G**, **L**, and $\mathbf{L}^{-1}$ matrices[20] and have reproduced

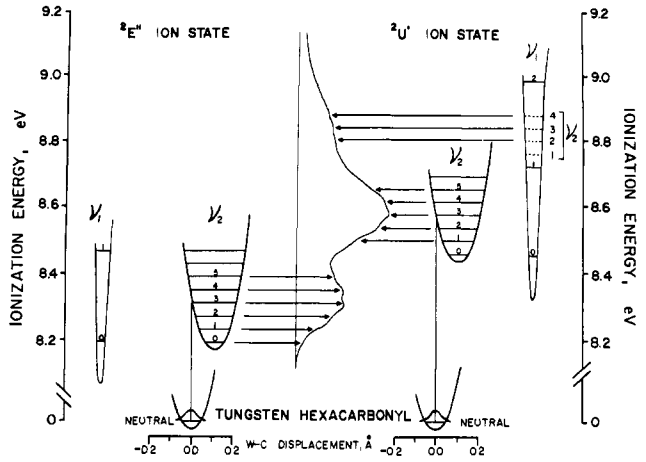

Figure 8. The ν_1 and ν_2 (a_{1g}) potential surfaces for the $W(CO)_6$ $^2E''$ and $^2U'$ ion states constructed from experimental data and ground-state normal mode analysis. The experimental ionization band is in the center of the figure.

the previous normal coordinate analysis of the a_{1g} vibrations of the neutral metal hexacarbonyls. Determination of the M–C distance in the positive ion also inherently includes two assumptions concerning the positive ion which should be noted. First, it assumes that the lowest ionization energy transition observed is to the $v = 0$ level (adiabatic). The most intense transition is then to the $v = 3$ level (vertical). If the adiabatic transition actually is not observed, then the vertical transition is to a vibrational quantum level higher than $v = 3$, and the change in metal–carbon bond distance is actually greater than we determine. Second, we assume that the shape of the metal–carbon a_{1g} potential well in the positive ion is the same as that in the ground state. Actually, we know that the vibrational frequency in the positive ion state is slightly lower than that in the neutral molecule, meaning that the actual positive ion potential well is slightly more broad. Figure 7 shows that this assumption also leads to an underestimate of the change in metal–carbon bond distance with t_{2g} ionization. The bond distance change that is determined in our present analysis might be viewed as a lower bound to the true value, although we do not expect that either of the assumptions we have mentioned will cause serious error.

The results of this analysis are illustrated in Figure 8. This figure is constructed with the correct scale between the vibrational potential wells of the ground state and the positive ions and matches the vibrational quantum levels with the observed vibrational progressions in the ionization band. The ν_2 (a_{1g}) normal mode potential well is plotted vs. the internal coordinate representing the W–C bond distances. The simple result from this analysis is that the W–C bond distances in the positive ion are displaced 0.10 Å from the distances in neutral $W(CO)_6$.

The lowered W–C vibrational frequency and increased W–C equilibrium bond length with removal of a single t_{2g} electron indicate the metal–carbon bond strengthening nature of an electron in these orbitals. One attractive feature of these observations is the symmetry separation of the σ- and π-bonding effects. Since the t_{2g} orbitals have only π symmetry interaction with the carbonyls, the direct deduction from these observations is that the predominantly metal t_{2g} orbitals are π bonding with respect to the carbonyls. It is difficult to attribute the observed ionization structure to any significant changes in the σ bonding.[21]

(20) (a) Wilson, E. B.; Decius, J. C.; Cross, P. C. "Molecular Vibrations"; McGraw-Hill: New York, 1955. (b) Jones, L. H. "Inorganic Vibrational Spectroscopy"; Marcel Dekker: New York, 1971. (c) Nakomoto, K. "Infrared and Raman Spectra of Inorganic and Coordination Compounds", 3rd ed.; Wiley: New York, 1978.

(21) Another effect of t_{2g} ionization is likely to be increased carbonyl σ donation to the more positive metal center, but increased σ bonding should tend to increase the M–C vibrational frequency rather than decrease it as is observed. The changed σ overlaps with the contracted metal d functions may also have an influence, but other experiments or calculations are necessary to determine if these changes are significant.

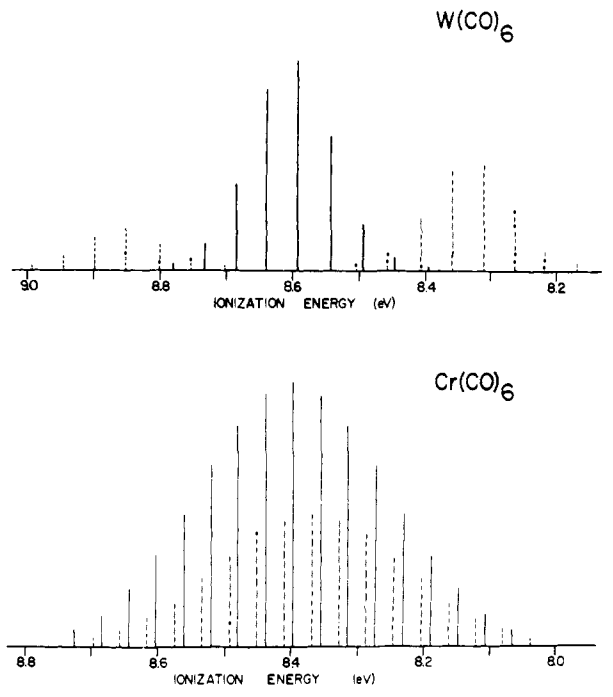

Figure 9. Schematic illustration of spin–orbit splitting and the vibrational detail for $W(CO)_6$ and $Cr(CO)_6$. The solid lines correspond to the $^2U'$ states and the dashed lines correspond to the $^2E''$ states. For $W(CO)_6$ the dotted lines centered at 8.85 eV correspond to the first excited ν_1 (a_{1g}) vibrational level of the $^2U'$ state.

The magnitude of the bond distance change should also be noted. The removal of one t_{2g} electron might be envisioned as the loss of one-sixth of the total metal–carbon π bond order in $W(CO)_6$. Since a typical W–C single bond is only 0.19 Å[22] longer than the W–CO bond (2.07 Å),[23] the 0.1 Å lengthening of the metal–carbon bonds with loss of one t_{2g} electron appears to be a proportionately large displacement. Actually, this is reasonable because the positive hole following t_{2g} ionization will be localized primarily on the metal, and this charge contracts the metal orbitals and further reduces the ability of the remaining t_{2g} electrons to back-bond to the carbonyls. Although operation of this positive ion effect has not been generally acknowledged in many previous photoelectron–vibronic studies of small molecules,[10-12] we believe that this relaxation effect may often be significant in the study of transition-metal species.[24]

B. $Cr(CO)_6$. The $^2T_{2g}$ band for $Cr(CO)_6$ is observed to have a subtle but distinct progression of six to seven elements with a frequency of $\sim$325 cm^{-1}. As has been shown, this progression is not as visually apparent as the ν_2 progression in the $W(CO)_6$ spectrum. This is most likely because of the small spin–orbit coupling parameter for the Cr atom in comparison to the large parameter for the W atom. A schematic representation of how the spin–orbit splitting affects observation of the ν_2 progression is shown in Figure 9. The large spin–orbit splitting of the W atom clearly separates the $^2U'$ and $^2E''$ ion states, giving well-separated progressions. An analogous representation for the $Cr(CO)_6$ band is constructed by using the known spin–orbit coupling parameter for Cr^0 and Cr^+.[18] The splitting of the $^2U'$ and $^2E''$ states in this case is one-half to two-thirds the magnitude of the ν_2 stretching frequency. This will intermesh the vibrational progressions for these two states and tend to diminish the fine structure on the ionization band. However, the progressions for the two states are in constant phase with each other, and therefore can be observed in the derivative, residual, and Fourier analyses.

The positive ion ν_2 frequency reduction by $\sim$60 cm^{-1} from the ground-state value indicates a considerable decrease in Cr–C bond order upon t_{2g} ionization. This represents a 15% frequency reduction compared to 10% for $W(CO)_6$. Additionally, the ν_2 progression in the $Cr(CO)_6$ spectrum is roughly twice as long as the $W(CO)_6$ ν_2 progression, as shown by both the overall width of the $Cr(CO)_6$ band compared to the $W(CO)_6$ bands and by the vibrational inflections that are observed. This indicates a greater displacement of the metal–carbon distances for $Cr(CO)_6$. We conservatively estimate the vertical transition to be to the $v = 6$ vibrational level, and from an analysis identical with that described for $W(CO)_6$, this gives the Cr–C bond displacements to be 0.14 Å.

Each of these observations is indicative of a metal–carbon bond strength (and bond distance) that is more sensitive to removal of a t_{2g} electron in the case of $Cr(CO)_6$ than in the case of $W(CO)_6$. This is supported by the trend in M–CO and M–C (single bond) distances from crystal structure determinations. As has already been mentioned, the W–C (single bond) distance is about 0.19 Å longer than the W–CO distance. In comparison, the Cr–C (single bond) distance is about 0.28 Å longer than the Cr–CO distance.[23,25] In both cases, the M–C bond distance in the $M(CO)_6$ positive ion, as determined by our vibrational analysis, is halfway between the M–CO and M–C (single bond) distances. The ionization data do not contain the explanation for this trend in bond distance changes. It could be that the σ bonding accounts for a greater portion of the bond in the case of $W(CO)_6$. This is consistent with the interpretation of the normal vibrational analysis.[3] It is also possible that the smaller Cr atom is less able to adapt its bonding following removal of the t_{2g} electron. A thorough theoretical investigation could perhaps shed light on this trend.

The $Cr(CO)_6$ ionization band does not show any signs of the ν_1 (predominantly CO) stretching mode that was observed in the $W(CO)_6$ spectrum. This is most probably the result of less delocalization of the t_{2g} density into the carbonyls in the case of $Cr(CO)_6$, although the longer ν_2 progression for $Cr(CO)_6$ may also obscure the short ν_1 progression.

C. $Mo(CO)_6$. The lack of a simple ν_2 progression in the $^2T_{2g}$ band of $Mo(CO)_6$ is considered to be the result of molybdenum's intermediate spin–orbit coupling ($\lambda \simeq 0.070$ eV).[18] This atomic parameter would be expected to split the $^2T_{2g}$ state by roughly 1.75–2.0 times the expected ν_2 frequency, thus causing a complex intermeshing of the vibronic detail on the resulting $^2E''$ and $^2U'$ states.

There are two observations concerning the $Mo(CO)_6$ $^2T_{2g}$ band that are of particular importance. First, the $Mo(CO)_6$ bandwidth is seen to be intermediate between the $Cr(CO)_6$ $^2T_{2g}$ bandwidth and the $W(CO)_6$ $^2E''$ or $^2U'$ bandwidths. This would indicate a ν_2 progression length intermediate between that seen in $Cr(CO)_6$ and $W(CO)_6$. Second the ν_1 C–O stretching mode is present in the $Mo(CO)_6$ spectrum, although its intensity is apparently much less than that in the corresponding $W(CO)_6$ spectrum. Both of these points would place $Mo(CO)_6$ between $Cr(CO)_6$ and $W(CO)_6$ in terms of t_{2g} delocalization.

Discussion

The ability to observe vibrational fine structure such as that reported in this paper requires a high signal-to-noise ratio, good resolution, and controlled stability in the instrumentation. The observation is also aided by data evaluation techniques that are common in other areas of spectroscopy. The fine structure is most clearly seen when only a single fundamental vibrational mode is excited (displacement of the normal mode potential well) by the ionization. We are finding that circumstances are suitable for observing vibrational fine structure in several different kinds of metal complexes,[26] apparently because the reasonably localized

(22) Forder, R. A.; Gale, G. D.; Prout, K. *Acta Crystallogr., Sect. B*: **1975**, *B31*, 307–309.
(23) Beach, N. A.; Gray, H. B. *J. Am. Chem. Soc.* **1968**, *90*, 5713.
(24) Calabro, D. C.; Lichtenberger, D. L. *Inorg. Chem.* **1980**, *19*, 1732 and references therein.
(25) Krausse, J.; Marx, G.; Schodl, G. *J. Organomet. Chem.* **1970**, *21*, 159.
(26) Calabro, D. C.; Hubbard, J. L.; Blevins, C. H.; Lichtenberger, D. L. *J. Am. Chem. Soc.* **1981**, *103*, 6839 (vibrational fine structure observed in $(\eta^5\text{-}C_5H_5)Re(CO)_3$); Blevins, C. H.; Lichtenberger, D. L., paper in preparation on vibrational fine structure in valence ionizations of molecules containing quadruple metal–metal bonds.

orbital density in many metal systems is conducive to activating only one or a few localized vibrations in the molecule. The vibrational structure may also be observed for removal of a delocalized electron if the molecule has appropriate symmetry, since it appears that a totally symmetric mode progression will dominate.[19] If the ionization is to a degenerate electronic state, it is helpful if the spin-orbit splitting is either very small or very large. Intermediate values of spin-orbit splitting (on the order of the vibrational spacings) can lead to more complicated vibrational patterns.

The vibrational fine structure can give a quantitative indication of the geometric structures of individual positive ion states, and this can provide unique information on the electronic structure, bonding, and stability of the molecule. In this case the bonding nature of the t_{2g} electrons between the metal and the carbonyls is evidenced by (1) the overall width and shape of the ionization bands, (2) the reduction of the ν_2 (a_{1g}) metal-carbon frequencies in the positive ions, (3) the intensity pattern of the ν_2 (a_{1g}) progressions, and (4) the presence of the ν_1 (a_{1g}) carbon-oxygen vibrational progression in the $Mo(CO)_6$ and $W(CO)_6$ spectra.

The interpretation of vibrational structure generally emphasizes only the bonding character of the orbital which is ionized. For transition-metal ionizations, it is important to also consider the charge reorganization of the remaining occupied orbitals in the positive ion.[24] For t_{2g} ionization from the metal hexacarbonyl, the effective increase in oxidation state of the metal center reduces the bonding ability of the remaining t_{2g} electrons. This serves to magnify the increase in metal-carbon bond length that occurs with removal of a single t_{2g} electron.

Acknowledgment. We wish to acknowledge the U.S. Department of Energy, Contract DE-ACOZ-80ER10746, the University of Arizona, and the donors of the Petroleum Research Fund, administered by the American Chemical Society, for partial support of this work. D.L.L. is an Alfred P. Sloan Fellow, 1979-1981.

Registry No. $W(CO)_6$, 14040-11-0; $Mo(CO)_6$, 13939-06-5; $Cr(CO)_6$, 13007-92-6.

Reactions of Metal-Metal Multiple Bonds. 8.[1] Forming Mo-Mo Quadruple Bonds by Reductive Elimination (Alkyl Group Disproportionation) in the Reactions of 1,2-$Mo_2R_2(NMe_2)_4$ Compounds (M≡M) with Carbon Dioxide and 1,3-Diaryltriazines

M. J. Chetcuti, M. H. Chisholm,* K. Folting, D. A. Haitko, and J. C. Huffman

Contribution from the Department of Chemistry and Molecular Structure Center, Indiana University, Bloomington, Indiana 47405. *Received February 2, 1981*

Abstract: Addition of CO_2 and 1,3-diaryltriazines to 1,2-$Mo_2R_2(NMe_2)_4$ compounds (M≡M), where R = CH_3 and $CH_2Si(CH_3)_3$, yields $Mo_2R_2(O_2CNMe_2)_4$ and $Mo_2R_2(NMe_2)_2(ArN_3Ar)_2$ compounds, respectively, with retention of the Mo≡Mo bond, whereas related reactions, where R = C_2H_5, $CH(CH_3)_2$, and *n*-, *sec*-, and *t*-C_4H_9, yield Mo-Mo quadruply bonded compounds $Mo_2(O_2CNMe_2)_4$ and $Mo_2(ArN_3Ar)_4$ by reductive elimination (alkyl group disproportionation) of alkene and alkane. Reactions involving the addition of CO_2 to the labeled compounds $Mo_2(CH_2CD_3)_2(NMe_2)_4$ and $Mo_2(CD_2CH_3)_2(NMe_2)_4$ yield CH_2DCD_3 + $CH_2{=}CD_2$ and CHD_2CH_3 + $CH_2{=}CD_2$, respectively. When a mixture of $Mo_2(CH_2CH_3)_2(NMe_2)_4$ and $Mo_2(CH_2CD_3)_2(NMe_2)_4$ and CO_2 reacted in benzene, the only deuterated products detected by ^2H NMR spectroscopy were $CH_2{=}CD_2$ and CH_2DCD_3. When mixtures of $Mo_2(CH_2CH_3)_2(NMe_2)_4$ and $Mo_2R_2(NMe_2)_4$ compounds (R = CH_3 and $CH_2Si(CH_3)_3$) in toluene-d_8 were allowed to react with CO_2 in sealed NMR tubes, only ethane and ethylene were evolved, whereas when mixtures of $Mo_2(CH_2CH_3)_2(NMe_2)_4$, $Mo_2(CH_2CH_3)(R)(NMe_2)_4$, and $Mo_2R_2(NMe_2)_4$ were allowed to react under similar conditions, the eliminated organic products were ethylene, ethane, and RH. These observations establish that reductive elimination occurs by an intramolecular reaction in which a β-hydrogen atom of one ethyl ligand is transferred to the α-carbon of the other ethyl or alkyl group. The insertion of CO_2 into Mo-NMe_2 bonds proceeds via an amine-catalyzed sequence: Me_2NH + CO_2 ⇌ Me_2NCOOH; Mo-NMe_2 + $HOOCNMe_2$ → MoO_2CNMe_2 + $HNMe_2$. The replacement of NMe_2 groups by either O_2CNMe_2 or ArN_3Ar ligands involves a protolysis which is common for metal dimethylamides: $M(NMe_2)_x + yLH \rightarrow M(NMe_2)_{x-y}L_y + yMe_2NH$. In the present instance, the reactions involving $Mo_2(CH_2CH_3)_2(NMe_2)_4$ have been shown to proceed through intermediates of formula $Mo_2(CH_2CH_3)_2(NMe_2)_2L_2$, where L = O_2CNMe_2 and ArN_3Ar (Ar = phenyl or *p*-tolyl). The carbamato intermediate has only been detected by ^1H NMR studies, but the *p*-tolyltriazenido compound has been isolated and structurally characterized. Crystal data for $Mo_2Et_2(NMe_2)_2(C_7H_7N_3C_7H_7)_2$: space group $P2_1/a$, a = 16.503 (4) Å, b = 23.116 (7) Å, c = 11.318 (3) Å, β = 88.15 (1)°, and Z = 4. The molecule has virtual, but not crystallographically imposed, C_2 symmetry. The Mo≡Mo bond is bridged by *cis*-triazenido ligands, which afford sufficient flexibility to allow a noneclipsed geometry with respect to each half of the molecule. Each molybdenum is coordinated to three nitrogen atoms and a carbon atom which lie roughly in a plane. Pertinent bond distances are Mo-Mo = 2.171 (1) Å, Mo-N (dimethylamide) = 1.95 (1) Å, Mo-C = 2.21 (1) Å, and Mo-N (triazenido) = 2.17 (1) Å and 2.251 (1) Å with the longer bond being trans to the Mo-NMe_2 group. Plausible mechanisms for the reductive-elimination sequence are presented and discussed in light of related organometallic reaction sequences.

The preparation[2] of an extensive series of 1,2-$M_2R_2(NMe_2)_4$ compounds (M≡M), where M = Mo and W and R = Me, Et, *i*-Pr, *n*-Bu, *sec*-Bu, *t*-Bu, CH_2CMe_3, and CH_2SiMe_3, provides the opportunity of studying the reactivity patterns of σ-alkyl groups[3]

(1) Chisholm, M. H.; Huffman, J. C.; Kirkpatrick, C. C. *Inorg. Chem.* **1981**, *20*, 871.

(2) Chisholm, M. H.; Haitko, D. A.; Folting, K.; Huffman, J. C. *J. Am. Chem. Soc.* **1981**, *103*, 4046.

0002-7863/82/1504-2138$01.25/0